

Particle size-dependent fluorescence properties of water-soluble organic compounds (WSOC) and their atmospheric implications on the aging of WSOC

5 Juanjuan Qin^{1,2}, Jihua Tan^{1*}, Xueming Zhou^{1,3}, Yanrong Yang¹, Yuanyuan Qin¹, Xiaobo Wang¹,
Shaoxuan Shi¹, Kang Xiao^{1*}, Xinning Wang²

¹College of Resources and Environment, University of Chinese Academy of Sciences, Beijing, 100049, China

²Guangzhou Institute of Geochemistry, Chinese Academy of Sciences, Guangzhou, 510640, China

³Faculty of Earth Resources, China University of Geosciences, Wuhan, 430074, China

Correspondence to: Jihua Tan (tanjh@ucas.ac.cn); Kang Xiao (kxiao@ucas.ac.cn)

10 **Abstract.** Water-soluble organic compounds (WSOC) play important roles in atmospheric particle formation, migration, and transformation processes. Size-segregated atmospheric particles were collected in a rural area of Beijing. Excitation-emission matrix (EEM) fluorescence spectroscopy was used to investigate the sources and optical properties of WSOC. Sophisticated data analysis on EEM data was performed to characteristically estimate the connections among particles of different sizes. WSOC concentrations and average fluorescence intensity (AFI) showed monomodal distribution in winter and bimodal 15 distribution in summer, with dominant mode in 0.26 - 0.44 μm size range in both seasons. The EEM spectra of WSOC varied with particle size, likely due to changing sources and/or chemical transformation of organics. Size distributions of fluorescence regional intensity (region III and V) and humification index (HIX) indicate that humification degree or aromaticity of WSOC was the highest in particle size range of 0.26-0.44 μm . The Stokes shift (SS) and the harmonic mean of the excitation and emission wavelengths (WH) reflected that π -conjugated systems were high in the same particle size range. The parallel factor 20 analysis (PARAFAC) results showed that humic-like substances were abundant in fine particles ($<1 \mu\text{m}$) and peaked at 0.26-0.44 μm . All evidences supported that the humification degree of WSOC increased with particle size in submicron mode ($<0.44 \mu\text{m}$) and then decreased gradually with particle size, which implied that condensation of organics occurred in submicron particles, resulting in the highest degree of humification in particle size range of 0.26-0.44 μm rather than in $<0.26 \mu\text{m}$. Synthetically analyzing 3-dimensional fluorescence data could efficiently reveal the secondary transformation processes of 25 WSOC.

1 Introduction

The environmental, health, and climate effects of atmospheric aerosol particles have been reiterated for many years (Pósfai and Buseck 2010; Burnett et al., 2018; Yan et al., 2020; Fan et al., 2020). Water-soluble organic compounds (WSOC) comprise 10% to 80% of organic compounds in atmospheric aerosols (Qin et al., 2018; Almeida et al., 2020; Cai et al., 2020). WSOC 30 play significant roles in cloud formation, solar irradiation, and atmospheric chemistry (Asa-Awuku et al., 2009; Duarte et al.,

2019). However, only 10% to 20% of the organic compounds have been structurally identified, and the majority of WSOC remain uncharacterized. Generally, WSOC mixture contains both aromatic nuclei and aliphatic chains (Decesari et al., 2001; Dasari et al., 2019), with functional groups or heteroatoms like hydroxyl, carboxyl, aldehyde, ketone, amino, and other nitrogen-containing groups (Duarte et al., 2007; Cai et al., 2020). Biomass burning and secondary transformation of organics 35 are believed to be the main sources of WSOC (Park et al., 2017; Xiang et al., 2017).

Many sophisticated analytical techniques have been developed to unveil the chemical structure of WSOC (Johnston and Kerecman 2019). Nuclear magnetic resonance (NMR) is a powerful tool in obtaining structures of organics (Stark et al., 2013; Duarte et al., 2015, 2020; Chalbot et al., 2016). Applications of other existing technologies used for identifying organics 40 structure include the electrospray ionization with ultrahigh-resolution Fourier-transform ion cyclotron resonance mass spectrometry (ESI-FT-ICR-MS), the proton transfer reaction mass spectrometry (PTR-MS), the Isotopic ratio mass spectroscopy (IRMS), and the accelerator mass spectroscopy (AMS), have been increasing because the requirement of further insight into organics in particulate matter (Cai et al., 2020; Mayorga et al., 2021), and source distinction of organic 45 emissions from fossil combustion or biogenic origin (Masalaite et al., 2018; Zhao et al., 2019; Huang et al., 2020).

The above-mentioned instruments are generally expensive to operate. In contrast, optical instruments like ultraviolet and 50 fluorescence spectrophotometers are relatively low-cost and efficient. Moreover, data generated by the optical instruments can provide quantitative and qualitative information simultaneously, which warrants their broad application on organics research, such as investigating WSOC and dissolved organic matter (DOM) in water (Hecobian et al., 2010; Qin et al., 2018; Xiao et al., 2016). 3-Dimensional excitation-emission matrix (EEM) fluorescence spectroscopy is an optical instrument that has been used 55 in analyzing atmospheric WSOC (Duarte et al., 2004; Fu et al., 2014). Fluorescence analysis can identify chromophoric organics like aromatics, protein, and other organic matters containing π -conjugated systems (Xiao et al., 2018; 2020). EEM spectrum has been implemented to visualize the fluorescence regions and identify possible categories of WSOC by characteristic of fluorescent regions (Duarte et al., 2004; Santos et al., 2009), and to study the aging of WSOC by examining the red or blue shift of fluorescence peaks (Lee et al., 2013; Fu et al., 2015; Vione et al., 2019). Fluorescence indices are important subsidiary approaches to statistically analyze EEM data (Qin et al., 2018; Yue et al., 2019), which are determined 55 by the chemical structure of pollutants (Andrade-Eiroa et al., 2013a).

Earlier studies have investigated size distributions of WSOC (Deshmukh et al., 2016; Frka et al., 2018), and more recent 60 studies have interests on the optical properties of size-segregated WSOC (Chen et al., 2019; Yue et al., 2019). Generally, the mass concentrations of WSOC show bimodal distributions with the dominant one in the accumulation mode (0.05-2 μ m) (Yu et al., 2004; Yu et al., 2016). Structural investigations on coal burning and biomass burning affected humic-like substances (a significant fraction of WSOC) in four size ranges found consistent organic species through all the size ranges, however, the absorption bands of aromatic groups were more intense compared to carboxylic groups in sub-3 μ m fractions (Park et al., 2017; Voliotis et al., 2017). Jang et al. (2019) comprehensively analyzed the structures of size-segregated humic-like substances extracted from PM_{2.5} in Songdo, South Korea? during periods of pre-, current and post-heating, and found that the chemical structures of HULIS changed with particle size. Liu et al. (2013) examined the light absorption properties of size-resolved

65 brown carbon (BrC) and methanol extracts in Georgia, and found that chromophores were predominant in the accumulation mode with an aerodynamic mean diameter of 0.5 μm . More recently, fluorescence properties of size-segregated ambient WSOC and bioaerosols were estimated in a coal burning city and a mountain site (Chen et al., 2019; Yue et al., 2019).

To date, comprehensive analysis of fluorescence properties of size-resolved aerosols is still very limited, with enormous information being hidden in the EEM spectra. The present study was designed to fill this knowledge gap by investigating the 70 fluorescence properties of WSOC in different particle sizes. Six stage size-segregated particle samples were collected in winter and summer in rural Beijing. Light-absorbing and fluorescent properties of size-segregated WSOC were obtained using the fast and efficient UV-Vis and fluorescence methods. A bunch of fluorescence indices, Stokes shift, and parallel factor analysis (PARAFAC) were performed to quantitatively disclosure the hidden connections and transformations of WSOC. Gary relational degree (GRD) was used to show the relations between particles.

75 2 Method

2.1 Sampling site

Size-segregated particle samples were collected by a 6-stage micro-orifice uniform deposit impactor (MOUDI), with aerodynamic cut-point diameters of 0.26, 0.44, 0.77, 1.4, 2.5, and 10 μm , respectively. Sample collection started at 8:00 a.m. till next 7:00 a.m., leaving 1 h for operation. All samples were collected on quartz filters (Whatman), which were prebaked for 80 5 hours (500°C) before sample collection, and were wrapped by aluminum foil and stored at -20°C.

A total of 20 sets of 6-stage size segregated aerosol samples were collected at a rural site in Huairou Distinct, Beijing, from 14 November to 30 December 2016 and from 30 June to 8 September 2017. The sample collection days were randomly selected and samples were later categorized according to the degree of air pollution. Winter sampling days covered six levels of air quality from excellent to severe pollution, while summer sampling days only covered good and moderate air quality. The air 85 quality index weighted 72h backward trajectories during the sampling period are exhibited in Figure 1.

2.2 Chemical analysis

Organic and elemental carbon (OC and EC) were determined by thermal/optical carbon analyzer (DRI), and the thermal evolution protocol IMPROVE (Interagency Monitoring of Protected Visual Environments) was adapted. Detailed information can be found in earlier studies (Cheng et al., 2009; Tan et al., 2016). The detection limit of OC and EC was 1.0 $\mu\text{g}/\text{m}^3$, as 90 quantified by filter and filter blank. QA and QC were performed by replicate analyses every 10 samples and the repeatability was better than 5%.

A quarter of the filter sample was ultrasonically extracted twice with 5 ml ultrapure water each time and mixed up after extraction. The extracts were then filtered through a 0.22 μm membrane filter to remove impurities (Xiang et al., 2017). The measurement of WSOC was performed by a TOC analyzer (Analytic Jena AG multi N/C3100, Germany).

95 The extraction procedures of water-soluble ions (WSIN) were similar to those of WSOC, but using 0.22 μm teflon filter to remove impurities. Ion chromatography (IC, Dionex ICS 900 and 1100) was used in the detection, with 8 WSIN species analyzed (Cl^- , NO_3^- , SO_4^{2-} , NH_4^+ , Na^+ , K^+ , Ca^{2+} and Mg^{2+}). The recovery (90%–110%) and reproducibility (relative standard deviation of each ion lower than 5%) of the ions were implemented as well.

2.3 Spectrophotometer Analysis

100 The extraction procedures of samples subject to fluorescence and ultraviolet-visible (UV-Vis) sampling were the same as for WSOC detection. The excitation-emission spectra were obtained by a fluorescence spectrophotometer (F-7000, Hitachi, Japan), and UV-Vis spectra by an ultraviolet spectrophotometer (UV-2401PC, Shimadzu, Japan). Briefly, the wavelength ranges of EEM were 200–400 nm for excitation and 250–500 nm for emission with 5 nm interval (Qin et al., 2018). UV-Vis was measured with a range of 200–500 nm with 5 nm interval. All EEM data in the present study were in Raman unit (R.U.).
105 The background signals, interfering signals (first- and second-order Rayleigh and Raman scatterings), and the inner-filter effects were removed by subtracting an EEM of blank and replaced with a band of missing values or inserting zeros outside the data area, as detailed in Bahram et al., (2006). Data correction and standardization followed procedures described in Xiao et al., (2016). As shown in Figure 2, the EEM spectra were partitioned into five regions (Birdwell and Engel 2010), and fluorescence regional integration (FRI) method was applied to examine the fluorescence intensities of the accordant region to 110 the total fluorescence intensity. Specific fluorescence intensity (SFI) was the fluorescence intensity divided by WSOC concentrations.

2.4 Data analysis

2.4.1 Fluorescent indices

115 Fluorescence indices based on intensity ratios may provide clues about the condensation state of WSOC. Humification index (HIX) was used to reflect the degree of humification (Kalbitz et al., 2000; Coble 2014).

$$\text{HIX} = \frac{\text{EEM}_{\text{Ex}254,\text{Em}435-480}}{\text{EEM}_{\text{Ex}254,\text{Em}300-345}} \quad (1)$$

Fluorescence is the light emission of a substance that has absorbed light or other electromagnetic radiation. The energy loss from fluorophore relaxing is expressed as Stokes Shift (SS), which was described in Xiao et al., (2019). In brief, SS is calculated according to equation (2) below, where λ_{Ex} is the excitation wavelength and λ_{Em} is the emission wavelength. The 120 harmonic mean of Ex/Em wavelength (WH) in equation (3) could represent the average energy level of excited states. Thus, SS and WH of each fluorescence intensity could be identified in an EEM spectrum.

$$\text{SS} = \frac{1}{\lambda_{\text{Ex}}} - \frac{1}{\lambda_{\text{Em}}} \quad (2)$$

$$\text{WH} = 2\left(\frac{1}{\lambda_{\text{Ex}}} + \frac{1}{\lambda_{\text{Em}}}\right)^{-1} \quad (3)$$

2.4.2 PARAFAC

125 PARAFAC model can decompose complex EEM spectra into several main components by statistical method. The excitation spectrum, emission spectrum, and scores of each component are as follows:

$$x_{ijk} = \sum_{f=1}^F a_{if} b_{jf} c_{kf} + \varepsilon_{ijk}, \quad i=1, \dots, I; \quad j=1, \dots, J; \quad k=1, \dots, K \quad (4)$$

130 Where x represents the fluorescence intensity, f is the number of components resolved by PARAFAC, a is proportional to the concentration of the f -th component, and b and c are the scaled estimating of the emission and excitation spectra. The subscript i is the sample number, and j and k represent emission and excitation wavelength, respectively. Before performing PARAFAC, all EEM data were normalized to unit norm to reduce concentration-related collinearity and avoid extremely different leverages (Wang et al., 2020). Tucker congruence coefficient (TCC) was determined for each excitation spectrum and emission spectrum, and a threshold of 0.95 was applied to confirm the spectral congruence. The model was determined by half-split validation.

135 2.4.3 Grey relational analysis (GRA)

Grey relational analysis (GRA) is part of the grey system theory proposed by Deng (1982), which can be used to describe the relative changes among factors in a system development process. The detailed calculation of grey relational degree (GRD) was explained in the supplementary information. Generally, in GRA, a reference line and one or a series of comparison sequences were selected, and GRD between the reference line and comparison line indicated the compactness degree. The 140 fluorescence properties of WSOC were considered as a grey system. Two sets of GRA were performed for the WSOC of each season. Firstly, considering the evolution of particle size as a changing system, larger particles might come from accumulation and transformation of smaller particles, especially for ultrafine particles. By setting data of particles smaller than 0.26 μm (WSOC concentrations, AFI or UV) as references and particles larger than 0.26 μm as comparisons, their affinities were analyzed by GRA. Secondly, the fluorescence spectra were generated by part of WSOC, setting the WSOC concentration as a 145 reference and AFI (or UV) as a comparison. The relations between WSOC and AFI for six stage particles were analyzed.

3 Results

3.1 Chemical compounds of size-segregated particles

Table 1 shows the size-segregated mass concentrations of WSIN, WSOC, and OC and their ratios generated from the data collected at a rural site in Beijing during winter and summer. WSOC showed a feature of monomodal in winter and bimodal 150 in summer, with a dominant mode between 0.26 to 0.44 μm in both seasons and a small secondary mode in particles larger than 1 μm in summer, indicating that carbonaceous species were mainly rich in fine particles (Huang et al., 2020). Contemporary reports by other researchers observed bimodal distribution of WSOC with two peaks located at 0.8 μm and 7 μm , respectively, in Shenzhen, China, and 0.4-0.5 μm and 2-3 μm in Gwangju, Korea (Yu et al., 2016; Huang et al., 2020).

155 The WSOC/OC ratios were 0.24 - 0.56 in winter and 0.16 - 0.31 in summer. These values were smaller than those previously reported for a polluted period in Beijing and those in the other cities in China (Tian et al., 2014; Wu et al., 2020). Earlier studies suggested higher WSOC/OC ratios in summer than winter (Xiang et al., 2017; Qin et al., 2018), which is in contrast to the results of the present study. Contrasting seasonal patterns in WSOC/OC ratios were also reported between urban and rural sites in Georgia, US (Zhang et al., 2012), which seemed to support our results presented above. The WSOC/OC ratios were higher in particles with an aerodynamic diameter smaller than 1.4 μm than in coarse mode (PM_{2.5-10}), which was accordant with findings previously reported for clear days in Beijing (Tian et al., 2016).

160

3.2 Excitation-emission spectra of size-segregated WSOC

165 The size segregated EEM spectra of winter and summer WSOC are depicted in Figure 2 (a) and (b), respectively, and their fluorescence intensities per unit WSOC (SFI) are in (c) and (d), respectively. The overall fluorescence peaks of EEM were mainly produced among regions II-V and the peaks were peak A, peak T, and peak M, which could be categorized as humic-
170 like, tyrosine-like, and oxygenated organic substances, respectively (Qin et al., 2018). The fluorophores first increased with increasing particle size and reached the highest intensities at particle sizes of 0.26-0.44 μm , and then decreased with increasing particle size in both seasons. Although the fluorescence peaks of WSOC were mainly produced at similar regions between the two seasons, the relative abundance was different (more quantitative analysis below). The aggregated fluorescence spectra of all size-segregated samples resembled the spectra of TSP and PM_{2.5} shown in Figure S1 with some subtle nuance in border shape (Chen et al., 2016a; Qin et al., 2018).

175 The detailed characteristics of EEM intensity could be found in SFI spectra. The SFI showed evident differences between fine and coarse mode particles in both seasons. The spectra of coarse mode WSOC covered a wide range of natural sources (according to our unpublished research), while the spectra of fine particles widely overlapped with that of PM_{2.5} in Figure S2 (matched with anthropogenic sources and secondary sources of our study), indicating that sources of WSOC affected its fluorescence properties. Besides, the SFI spectra showed a clear blue shift within regions I to III with increasing particle size in winter, and showed humble variations in summer.

180 Figure 3 shows the size distribution of WSOC and its average fluorescence intensity (AFI) in the two seasons. AFI showed monomodal distribution with peaks in particle sizes of 0.26-0.44 μm in winter, and bimodal distribution in summer, which was accordant with the size distribution of WSOC. AFI/WSOC ratios could represent the overall average fluorescence density of WSOC (Xiao et al., 2016). The AFI/WSOC ratios ranged from 0.22 to 0.57 in winter and from 0.18 to 0.34 in summer. These values were higher than that in the industrial city of Lanzhou (Qin et al., 2018). Our unpublished research found that the AFI/WSOC ratios were lower than 0.2 for anthropogenic source samples.

185 Fluorescence regional integration (FRI) was calculated to quantify the relative strength of fluorescence intensity on regions I-V, represented by FRI1-FRI5 (Figure 4). FRI I and FRI II (protein-like species) increased with increasing particle size and peaked at coarse mode in winter. FRI III and FRI V (HULIS) were mainly abundant in fine particles. FRI IV (microbial related species) showed little variations in particle size range of 0.26-2.5 μm , but decreased with particle size from 2.5 to 10 μm . In

summer, the sum of FRI I to FRI III increased with particle size increasing, peaked at 1.4 μm and decreased with particle sizes from 1.4 to 10 μm . FRI IV showed reverse tendencies and decreased with particle size in the range of 0.26 to 1.4 μm , and increase in the particle size range of 1.4 - 10 μm . FRI V didn't have a clear tendency but they showed high portions among 190 0.26 to 0.44 μm and 0.77 to 1.4 μm .

3.3 Fluorescent indices and properties associated with fluorescence mechanisms

Inclusive information was stored in EEM spectra, with some regularities being extracted by performing division of fluorescence intensities between wavelengths. Humification index (HIX) represents the humification degree or aromaticity of fluorescent organics. Peak T/Peak C, the ratio between tryptophan and humics, can reflect the biodegradability of organics.

195 Some other fluorescence indices are listed in Table S1. Figure 5 shows the size distribution of HIX and Peak T/Peak C ratio. HIX showed monomodal distribution peaking between 0.26 to 0.44 μm in summer and 0.44 to 0.77 μm in winter, indicating the aromaticity of size-segregated WSOC increased first and then decreased afterwards with increasing particle size. Peak T/Peak C ratio increased gradually with increasing particle size in winter, while in summer it decreased first in fine particles 200 and then increased with particle size. Peak T/Peak C peaked at coarse mode in both seasons, indicating that fluorescent microbial related species likely existed in large atmospheric particles. It was reported that biogenic oxygenated organics are more inclined to adhere to coarse mode particles (Huang et al., 2020).

Stokes shift (SS) is the energy loss of fluorophore relaxation, which might be associated with the π -conjugated system and electron cloud density (Lakowicz, 2006). High SS values indicate greater energy loss due to relaxation in the excited states. Organic compounds having larger π -conjugation scales are possibly exhibiting high fluorescence intensity in the high SS 205 region (Xiao et al., 2020). Xiao et al., (2019) found that SS near 1.2 μm^{-1} is an important border of hydrophobic and hydrophilic components. Hydrophobic fractions tend to have higher intensity in SS >1.2 , possibly as a result of the large scale of the π conjugated system. In contrast, hydrophilic fractions usually have ionogenic groups bond with fluorescent aromatics reduced π -conjugated systems, hence, leading to high fluorescence intensities existing on both sides of SS of 1.2. Note that the same research also reported earlier that hydrophobic fractions tended to present fluorescence peaks at SS >1 (Xiao et al., 2016).

210 Thus, the ratios of fluorescence intensity in high SS (>1.1) are calculated as follows:

$$\eta_{SS>1.1} = \frac{\sum_{Ex} \sum_{Em} I|_{SS>1.1}}{\sum_{Ex} \sum_{Em} I} \quad (7)$$

The harmonic mean of the excitation and emission wavelengths (WH) reflects the average energy level of the excited states. On a large π -conjugated system, the electron in the ground state needs relatively low excitation energy jumping to the excited state (Berberan-Santos and Valeur, 2012). The ratios of fluorescence intensity in low energy state (WH >320) are calculated as 215 follows:

$$\eta_{WH>320} = \frac{\sum_{Ex} \sum_{Em} I|_{WH>320}}{\sum_{Ex} \sum_{Em} I} \quad (8)$$

Size-segregated SS, average SS, and $\eta_{SS>1.1}$ are shown in Figure S4 and Figure S5. SS of all particle sizes showed similar distributions, in terms of the consistency of fluorescence energy for WSOC. The intensities for SS <1.1 were of the same level

as those for $SS > 1.1$, indicating the predominance of hydrophilic fluorescent contents in WSOC. The average SS showed
220 unobtrusive variations with increasing particle size in both seasons, and $\eta_{SS > 1.1}$ was slightly higher in particle sizes $< 1.4 \mu\text{m}$ than other particle size, in winter. $\eta_{WH > 320}$ tended to increase from particle size 0.26 to 0.44 μm and then decrease afterwards in both winter and summer (Figure 5c), indicating existence of a large scale π conjugated system or high π -electron density around 0.44 μm , and decreased with particle size in 0.44 to 10 μm .

3.4 EEM fluorophore revealed by classification of PARAFAC results

225 PARAFAC is a mathematical method capable of separating chemically independent but spectrally overlapping fluorescence components, based on the assumption that EEM spectra are independent, liner related and additive (Murphy et al., 2011). Several prior studies have been carried out using the PARAFAC method to investigate fluorescent WSOC in atmospheric aerosols (Pohlker et al., 2012; Chen et al., 2019; Yue et al., 2019). Results showed that bioaerosols exhibited high bimodal signals at excitation wavelength 275nm and emission wavelength 320nm, which is sorted as protein-like organic matter. In a
230 typical coal burning city of China, fluorophores emerging at excitation wavelength 230-250nm and emission wavelength 380-410 nm were associated with humic-like substances with large molecular weight.

The present study conducted PARAFAC analysis for winter and summer samples separately to reveal seasonal dependent EEM spectra. Three components were extracted from winter EEM spectra, including C1 defined as HULIS-1, C2 representing a protein-like component, and C3 defined as HULIS-2 (Chen et al., 2016b). However, only two recognizable components were
235 identified in summer, with C1 characterized as HULIS-1 and C2 as protein-like components. Component C3 in summer EEM spectra was of no physical significance (multiple emission peak points at one single excitation wavelength) and characterized as a noise signal.

The portions of the extracted components are also shown in Figure 6 together with PARAFAC results. Protein-like compounds were more abundant in particles larger than 2.5 μm in both seasons (37%-40% in winter and 20%-21% in summer),
240 and HULIS showed higher fractions in fine mode than coarse mode particles in both seasons, which quantitatively demonstrated that microbial related WSOC more likely existed in large particles and HULIS was rich in fine particles. The ratios of HULIS-1 / HULIS-2 in winter were higher in fine particles with an aerodynamic diameter of 0.44-2.5 μm than in ultrafine particles ($< 0.26 \mu\text{m}$) or coarse mode particles. HULIS-2 was likely freshly emitted fluorescent WSOC and HULIS-1 exhibited fluorescent characteristics of oxidized HULIS (Vione et al., 2019). The low HULIS-1 / HULIS-2 ratios in ultrafine
245 and coarse mode particles might be due to abundant sources of freshly emitted WSOC.

3.5 Specific relations among size-segregated WSOC and fluorescence properties weighted by Gary Relational Degree (GRD)

GRA method is suitable for solving problems with complicated interrelationships between multiple factors and variables (Morán et al., 2006). It has been used for solving environmental issues (Kuo et al., 2008; Xu et al., 2011; You et al., 2017).

250 GRA was performed in the present study considering that atmospheric particles can be treated as a grey system for their high complexity and indeterminacy.

High GRD represents high connection between referencing and comparing factors. By setting WSOC (or AFI and UV) of particles $<0.26\text{ }\mu\text{m}$ as references and those of larger particles as comparisons, relations among particle sizes can be depicted by GRD of size-segregated WSOC (or AFI and UV), as shown in Figure 7(a) for winter samples and Figure 7(b) for summer samples. In winter, GRD_{0.44} to GRD_{2.5} showed a downward tendency varying from 0.88 to 0.76 for WSOC and 0.88 to 0.78 for AFI, indicating that WSOC concentration and AFI gradually deviating from their original situation with increasing particle size. In summer, GRD_{0.44} to GRD_{2.5} showed little variations with average values at 0.64 for WSOC and 0.73 for AFI, but decreased in GRD₁₀, indicating that WSOC in particles larger than $0.26\text{ }\mu\text{m}$ had little inheritance from the primal fine particle.

The relations between WSOC and AFI and average UV (referred to as UV below) of different particles are shown in Figure 260 7 (c) and (d) for winter and summer, respectively. AFI and UV showed high GRD in both seasons for all particle sizes (with average GRD >0.9), indicating that fluorescence intensity and light absorption were closely connected with WSOC concentration. However, clear variations of GRD were observed with increasing particle size with contrasting patterns to those 265 of fluorescence indices. Thus, it was speculated that these variations were resulted from secondary transformation of WSOC, as indicated by fluorescence indices. Besides, GRD strongly negatively correlated with estimated secondary organic carbon (SOC) concentration with a correlation efficient r of -0.64 ($p<0.000$) in winter and -0.63 in summer. The lowest GRD was found for particle sizes of $0.26\text{--}0.44\text{ }\mu\text{m}$. The high AFI, large π -conjugation scale, rich HULIS, and low GRD in this particle size range indicated that fluorescent WSOC of these particles was highly affected by secondary processes. Thus, GRD between WSOC and AFI could serve as an indicator of secondary formation.

4 Discussion

270 By characteristically analyzing the fluorescent properties of size-segregated WSOC, we have gained a better understanding of the hidden relations between fluorescence and WSOC concentration, the possible evolution of fluorescence properties during particle size growth, and the source distinction of fluorescent WSOC between fine and coarse particles.

Accordant with earlier reports, the fluorescence intensities positively correlated with WSOC concentrations in both winter and summer (Spearman's $r>0.8$, $p<0.001$) (Qin et al., 2018; Chen et al., 2019). The size distributions of AFI kept in step with 275 those of WSOC concentrations and showed monomodal distributions in winter and bimodal distributions in summer, peaking in particle sizes between 0.26 to $0.44\text{ }\mu\text{m}$ (Figure 2 (a) and (b)). The EEM spectra of size-segregated WSOC mainly exhibited among regions II-V and blue-shifted with increasing particle size (0.44 to $10\text{ }\mu\text{m}$).

The SFI spectra (fluorescence intensity per unit WSOC) showed different properties in different seasons or particle sizes. The size-segregated AFI/WSOC ratios were relatively high in fine particles with sizes between 0.26 to $1.4\text{ }\mu\text{m}$ (mainly affected 280 by anthropogenic sources and secondary process) and low in large particles ($\text{PM}_{2.5}$), but all were higher than those of source samples. Freshly emitted WSOC from the source sample contain more unsaturated groups like aromatics and have lower O/C

than the aged ones (Zhang et al., 2018, Cai et al., 2020). Substitution and oxidation reactions of ambient organics might widen the delocalization of π electrons and reduce the excitation energy, thereby resulting in a redshift of EEM spectra (Kalberer et al., 2004). The specific fluorescence area was widened in ambient sample and thus had a higher AFI/WSOC ratio when 285 WSOC concentrations were at a comparable level. Continuous oxidation of organics may break up the π system of organics and extinct fluorescence (Zanca et al., 2017). It could be inferred that ambient WSOC tended to exhibit higher AFI/WSOC ratios, while both freshly emitted WSOC and completely oxidized WSOC could lead to lower AFI/WSOC values.

The fluorescence indices showed clear particle size-dependent changes and vague seasonal variations. The same tendencies, i.e., increased first, peaked in particle size between 0.22 to 0.44 μm , and then decreased with particle size, were observed in 290 fluorescence indices of HIX and $\eta_{\text{WH}>320}$, indicating that the π -conjugated system of WSOC increased and then decreased with particle size. Besides, in the EEM spectra, peak M was strong in particle sizes lower than 0.77 μm and bleached in larger particles, and peak A blue-shifted with increasing particle size. Contemporary research also found that aromatic secondary 295 organic aerosol increased during the haze period (Yu et al., 2019). Besides, it was noticed that HIX and WSOC/OC showed similar size distributions except for larger peaking particle size of WSOC/OC values comparing to HIX. Because the fine particles with relatively large sizes could long exist in atmospheric environment, the WSOC/OC ratios increase gradually, however, the oxidation process could also cause fluorescence quenching and lead to the decrease of HIX (Vione et al., 2019). Thus, HIX peaked in smaller particle size comparing to WSOC/OC.

All evidence on EEM spectra and fluorescence indices discussed above suggested that the aging of WSOC might have experienced evolution processes of particle size changes. In the process of particle size increase, fluorescence and π -conjugated 300 system increased and peaked between 0.22 to 0.44 μm , and peak M sparkled. Two possible mechanisms were proposed to explain this phenomenon. The first one was that heterogeneous polymerization of gas and liquid phase organics enlarged the delocalization of π electrons and led to the increase of fluorescence (Kalberer et al., 2004). De Laurentiis et al. (2013) found that the triplet state of 1-nitronaphthalene directly reacted with phenol and formed biopolymer transformation intermediates in the liquid phase, and the fluorescence spectra shifted to peak “M” during irradiation. The second one was that during oxidation 305 processes of organics in small particles, oxygen heteroatomic rings formed or chromophoric groups like $-\text{NO}_2$ and $-\text{OH}$ added to the fluorescent organics, which both could increase the π -conjugated system. Lee et al., (2014) observed that fluorescence intensity of secondary organic aerosol produced by high- NO_x photooxidation of naphthalene (NAP SOA) increased when they were solar irradiated. In the process of particle size decrease, fluorescence decreased with increasing particle size and peak M dribbled away. This might be because further oxidation process gradually broke up the aromatic rings or unsaturated bonds in 310 organic matters and fluorescence quenched. Laboratory results also confirmed that after a long period of irradiation the fluorescence intensity of fluorescent organic decreased eventually (De Laurentiis et al., 2013, Lee et al., 2014).

PARAFAC results showed that HULIS was rich in fine particles and protein-like compounds were rich in coarse particles in both seasons, which were accordant with earlier reports (Chen et al., 2019; Huang et al., 2020). In winter, the wavelength of HULIS-1 was slightly higher than that of HULIS-2. The EEM spectra of HULIS-1 observed in the present study were 315 similar to the PARAFAC results of highly oxygenated species, while those of HULIS-2 to less oxygenated species reported in

Chen et al (2016b) on the chromophoric WSOC. Only HULIS-1 was distinguished in summer in the present study, which could be allocated to highly oxygenated species.

The particle size dependent variations of HULIS-1 reflected that the contents of the highly oxygenated species in WSOC increased first, peaked between 0.26 to 0.44 μm , and then decreased with particle size, which cogently confirmed the size-320 dependent chemical composition of WSOC. Such a finding is consistent with the trend of O/C ratio in size-resolved samples in Shenzhen in a winter (Huang et al., 2020). The variations of HULIS-1 further suggested that secondary processes were active during the particle formation process, which confirmed that GRD value can be applied as an indicator of the aging state of WSOC.

5 Conclusions and Implications

325 In this study, a 6 stage MOUDI sampler was adopted to collected size-segregated samples of aerosol particles in a rural site of Beijing. The WSOC concentrations, UV absorption, fluorescence properties, and the energy information of fluorophores of different particle sizes were analyzed. PARAFAC method was used to decompose the mixture of fluorophores. The connections between WSOC and AFI of different particles were analyzed by grey relational degree (GRD). WSOC and AFI showed monomodal distributions in winter and bimodal distributions in summer. The fluorescence efficiency (AFI/WSOC) 330 was higher in winter than summer and higher in particle sizes $<1.4\text{ }\mu\text{m}$ than in larger particles. The variations of Fluorescence indices HIX and Peak T/Peak C ratio, and the $\eta_{\text{WH}>320}$ indicated that the aromaticity or π -conjugated systems of WSOC increased in ultrafine particles ($<0.44\text{ }\mu\text{m}$) and decreased in the afterwards particle sizes. PARAFAC results showed that HULIS was rich in fine mode and protein-like sources were rich in large particles. The GRD results suggested that fluorescent WSOC in particle sizes between 0.26 to 0.44 μm were highly affected by secondary sources.

335 The SFI spectra of coarse mode WSOC were relatively stable and could serve as a reference for identifying natural sources of WSOC. The AFI/WSOC ratio in ambient WSOC showed vast distinction from that of source samples, and it could be used as a potential indicator of the oxidation degree of secondary WSOC. More research on AFI/WSOC ratio is recommended for generating representative values for different sources and transformation processes.

340 The particle size dependent variations of fluorescent characteristics suggested the potential applications of the fluorescence method in investigating the aging processes of WSOC. Along with fluorescence indices, extensive information could be addressed in an EEM spectrum including the fluorescence intensities, the humification degree, the energy state and the sources of WSOC. If the connections between fluorescence property and chemical structure of organic matter are well understood, it might be possible to only use EEM data to understand the oxidation states of organics. The seasonal and particle size dependant 345 variations of fluorescent of WSOC suggested that the sources and transformations of anthropogenic sources were quite different in winter and summer, secondary processes could induce fluorescence variations of WSOC. Therefore, future research could take effort to research the fluorescence characteristic of secondary WSOC.

Author contribution: JT and KX designed the experiments, JQ collected all samples, JQ and YY carried out the experiments. JQ performed data analysis and indices calculation and KX supervised. YQ, XW, and SS provided advice on data analysis and 350 literal problems. XZ, XM, KX, and JT provided technical consultations about article writing. JQ prepared the manuscript with contributions from all co-authors.

Acknowledge: This work was supported by the National Natural Science Foundation of China (Grant Nos. 41675127, 41475116). We also appreciate the valuable advice from the editor who greatly improved the manuscript.

355

Disclaimer Competing interests: The authors declare that they have no conflict of interest.

References

Almeida, A. S., Ferreira, R. M. P., Silva, A. M. S., Duarte, A. C., Neves, B. M. and Duarte, R.: Structural features and 360 inflammatory effects of water-soluble organic matter in inhalable fine urban air particles, Environ Sci Technol, 54, 1082–1091, <https://doi.org/10.1021/acs.est.9b04596>, 2020.

Andrade-Eiroa, Á., Canle, M. and Cerdá, V.: Environmental applications of excitation-emission spectrofluorimetry: An in-depth review I, Applied Spectroscopy Reviews, 48, 1-49, <https://doi.org/10.1080/05704928.2012.692104>, 2013.

Asa-Awuku, A., Engelhart, G. J., Lee, B. H., Pandis, S. N. and Nenes, A.: Relating CCN activity, volatility, and droplet growth 365 kinetics of β -caryophyllene secondary organic aerosol, Atmos. Chem. Phys., 9, 795-812, <https://doi.org/10.5194/acp-9-795-2009>, 2009.

Bahram, M., Bro, R., Stedmon, C. and Afkhami, A.: Handling of Rayleigh and Raman scatter for PARAFAC modeling of fluorescence data using interpolation, J. Chemometr., 20, 99-105, <https://doi.org/10.1002/cem.978>, 2006.

Berberan-Santos, M. N. and Valeur, B.: Molecular fluorescence: Principles and Applications, Second Edition, Wiley-VCH, 370 Germany, <https://doi.org/10.1002/9783527650002.index>, 2012.

Birdwell, J. E. and Engel, A. S.: Characterization of dissolved organic matter in cave and spring waters using UV-Vis absorbance and fluorescence spectroscopy, Org. Geochem., 41, 270-280, <https://doi.org/10.1016/j.orggeochem.2009.11.002>, 2010.

Burnett, R., Chen, H., Szyszkowicz, M., Fann, N., Hubbell, B., Pope, C. A., Apte, J. S., Brauer, M., Cohen, A., Weichenthal, 375 S., Coggins, J., Di, Q., Brunekreef, B., Frostad, J., Lim, S. S., Kan, H., Walker, K. D., Thurston, G. D., Hayes, R. B., Lim, C., Turner, M. C., Jerrett, M., Krewski, D., Gapstur, S. M., Diver, W. R., Ostro, B., Goldberg, D., Crouse, D. L., Martin, R. V., Peters, P., Pinault, L., Tjepkema, M., van Donkelaar, A., Villeneuve, P. J., Miller, A. B., Yin, P., Zhou, M., Wang, L., Janssen, N. A. H., Marra, M., Atkinson, R. W., Tsang, H., Quoc Thach, T., Cannon, J. B., Allen, R. T., Hart, J. E., Laden, F., Cesaroni, G., Forastiere, F., Weinmayr, G., Jaensch, A., Nagel, G., Concin, H. and Spadaro, J. V.: Global estimates of mortality

380 associated with long-term exposure to outdoor fine particulate matter, Proc. Natl. Acad. Sci. USA, 115, 9592, <https://doi.org/10.1073/pnas.1803222115>, 2018.

Cai, J., Zeng, X., Zhi, G., Gligorovski, S., Sheng, G., Yu, Z., Wang, X. and Peng, P. a.: Molecular composition and photochemical evolution of water-soluble organic carbon (WSOC) extracted from field biomass burning aerosols using high-resolution mass spectrometry, Atmos. Chem. Phys., 20, 6115-6128, <https://doi.org/10.5194/acp-20-6115-2020>, 2020.

385 Chalbot, M. G., Chitranshi, P., da Costa, G. G., Pollock, E. and Kavouras, I. G.: Characterization of water-soluble organic matter in urban aerosol by ¹H-NMR spectroscopy, Atmos. Environ., 128, 235-245, <https://doi.org/10.1016/j.atmosenv.2015.12.067>, 2016.

Chen, Q., Mu, Z., Song, W., Wang, Y., Yang, Z., Zhang, L. and Zhang, Y. L.: Size-resolved characterization of the chromophores in atmospheric particulate matter from a typical coal-burning city in China, J. of Geophys. Res.: Atmos, 124, 390 10546-10563, <https://doi.org/10.1029/2019jd031149>, 2019.

Chen, Q. C., Ikemori, F. and Mochida, M.: Light absorption and excitation-emission fluorescence of urban organic aerosol components and their relationship to chemical structure, Environ. Sci. Technol., 50, 10859-10868, <https://doi.org/10.1021/acs.est.6b02541>, 2016a.

Chen, Q. C., Miyazaki, Y., Kawamura, K., Matsumoto, K., Coburn, S., Volkamer, R., Iwamoto, Y., Kagami, S., Deng, Y. G., 395 Ogawa, S., Ramasamy, S., Kato, S., Ida, A., Kajii, Y. and Mochida, M.: Characterization of chromophoric water-soluble organic matter in urban, forest, and marine aerosols by HR-ToF-MS analysis and excitation emission matrix spectroscopy, Environ. Sci. Technol., 50, 10351-10360, <https://doi.org/10.1021/acs.est.6b01643>, 2016b.

Cheng, Y., He, K. B., Duan, F. K., Zheng, M., Ma, Y. L. and Tan, J. H.: Measurement of semivolatile carbonaceous aerosols and its implications: A review, Environ. Int., 35, 674-681, <https://doi.org/10.1016/j.envint.2008.11.007>, 2009.

400 Coble, P.: Aquatic organic matter fluorescence, New York, US, Cambridge University Press, <https://doi.org/10.1017/CBO9781139045452>, 2014.

Coble, P. G.: Characterization of marine and terrestrial DOM in seawater using excitation emission matrix spectroscopy, Mar. Chem., 51, 325-346, [https://doi.org/10.1016/0304-4203\(95\)00062-3](https://doi.org/10.1016/0304-4203(95)00062-3), 1996.

Dasari, S., Andersson, A., Bikkina, S., Holmstrand, H., Budhavant, K., Satheesh, S., Asmi, E., Kesti, J., Backman, J., Salam, 405 A., Bisht, D. S., Tiwari, S., Hameed, Z. and Gustafsson, Ö.: Photochemical degradation affects the light absorption of water-soluble brown carbon in the South Asian outflow, Sci. Adv., 10, <https://doi.org/10.1126/sciadv.aau8066>, 2019.

De Laurentiis, E., Sur, B., Pazzi, M., Maurino, V., Minero, C., Mailhot, G., Brigante, M. and Vione, D.: Phenol transformation and dimerisation, photosensitised by the triplet state of 1-nitronaphthalene: A possible pathway to humic-like substances (HULIS) in atmospheric waters, Atmos. Environ., 70, 318-327, <https://doi.org/10.1016/j.atmosenv.2013.01.014>, 2013.

410 Decesari, S., Facchini, M. C., Matta, E., Lettini, F., Mircea, M., Fuzzi, S., Tagliavini, E. and Putaud, J. P.: Chemical features and seasonal variation of fine aerosol water-soluble organic compounds in the Po Valley, Italy, Atmos. Environ., 35, 3691-3699, [https://doi.org/10.1016/s1352-2310\(00\)00509-4](https://doi.org/10.1016/s1352-2310(00)00509-4), 2001.

Deng, J.-L.: Control problems of grey systems, *Syst. Control Lett.*, 1, 288-294, [https://doi.org/10.1016/S0167-6911\(82\)80025-X](https://doi.org/10.1016/S0167-6911(82)80025-X), 1982.

415 Deshmukh, D. K., Kawamura, K. and Deb, M. K.: Dicarboxylic acids, omega-oxocarboxylic acids, alpha-dicarbonyls, WSOC, OC, EC, and inorganic ions in wintertime size segregated aerosols from central India: Sources and formation processes, *Chemosphere*, 161, 27-42, <https://doi.org/10.1016/j.chemosphere.2016.06.107>, 2016.

Duarte, R., Pineiro-Iglesias, M., Lopez-Mahia, P., Muniategui-Lorenzo, S., Moreda-Pineiro, J., Silva, A. M. S. and Duarte, A. C.: Comparative study of atmospheric water-soluble organic aerosols composition in contrasting suburban environments in 420 the Iberian Peninsula Coast, *Sci. Total. Environ.*, 648, 430-441, <https://doi.org/10.1016/j.scitotenv.2018.08.171>, 2019.

Duarte, R., Pio, C. A. and Duarte, A. C.: Synchronous scan and excitation-emission matrix fluorescence spectroscopy of water-soluble organic compounds in atmospheric aerosols, *J. Atmos. Chem.*, 48, 157-171, <https://doi.org/10.1023/B:JOCH.0000036845.82039.8c>, 2004.

Duarte, R., Santos, E. B. H., Pio, C. A. and Duarte, A. C.: Comparison of structural features of water-soluble organic matter 425 from atmospheric aerosols with those of aquatic humic substances, *Atmos. Environ.*, 41, 8100-8113, <https://doi.org/10.1016/j.atmosenv.2007.06.034>, 2007.

Duarte, R. M. B. O., Duan, P., Mao, J., Chu, W., Duarte, A. C. and Schmidt-Rohr, K.: Exploring water-soluble organic aerosols structures in urban atmosphere using advanced solid-state ^{13}C -NMR spectroscopy, *Atmos. Environ.*, 230, 117503, <https://doi.org/10.1016/j.atmosenv.2020.117503>, 2020.

430 Duarte, R. M. B. O., Freire, S. M. S. C. and Duarte, A. C.: Investigating the water-soluble organic functionality of urban aerosols using two-dimensional correlation of solid-state ^{13}C -NMR and FTIR spectral data, *Atmos. Environ.*, 116, 245-252, <https://doi.org/10.1016/j.atmosenv.2015.06.043>, 2015.

Fan, J., Rosenfeld, D., Zhang, Y., Giangrande, S. E., Li, Z., Machado, L. A. T., Martin, S. T., Yang, Y., Wang, J., Artaxo, P., Barbosa, H. M. J., Braga, R. C., Comstock, J. M., Feng, Z., Gao, W., Gomes, H. B., Mei, F., Pöhlker, C., Pöhlker, M. L., 435 Pöschl, U. and Souza, R. A. F. d.: Substantial convection and precipitation enhancements by ultrafine aerosol particles, *Science*, 359, 8, <https://doi.org/10.1126/science.aan8461>, 2020.

Frka, S., Grgić, I., Turšič, J., Gini, M. I. and Eleftheriadis, K.: Seasonal variability of carbon in humic-like matter of ambient size segregated water-soluble organic aerosols from urban background environment, *Atmos. Environ.*, 173, 239-247, <https://doi.org/10.1016/j.atmosenv.2017.11.013>, 2018.

440 Fu, P., Kawamura, K., Chen, J. and Miyazaki, Y.: Secondary production of organic aerosols from biogenic VOCs over Mt. Fuji, Japan, *Environ Sci Technol*, 48, 8491-8497, <https://doi.org/10.1021/es500794d>, 2014.

Fu, P., Kawamura, K., Chen, J., Qin, M., Ren, L., Sun, Y., Wang, Z., Barrie, L. A., Tachibana, E., Ding, A. and Yamashita, Y.: Fluorescent water-soluble organic aerosols in the High Arctic atmosphere, *Sci Rep*, 5, <https://doi.org/10.1038/srep09845>, 2015.

445 Hecobian, A., Zhang, X., Zheng, M., Frank, N., Edgerton, E. S. and Weber, R. J.: Water-Soluble Organic Aerosol material and the light-absorption characteristics of aqueous extracts measured over the Southeastern United States, *Atmos. Chem. Phys.*, 10, 5965-5977, <https://doi.org/10.5194/acp-10-5965-2010>, 2010.

450 Huang, X. F., Dai, J., Zhu, Q., Yu, K. and Du, K.: Abundant biogenic oxygenated organic aerosol in atmospheric coarse particles: plausible sources and atmospheric implications, *Environ. Sci. Technol.*, 54, 1425-1430, <https://doi.org/10.1021/acs.est.9b06311>, 2020.

Jang, K.-S., Choi, A. Y., Choi, M., Kang, H., Kim, T.-W. and Park, K.-T.: Size segregated chemical compositions of HULISs in ambient aerosols collected during the winter season in Songdo, South Korea, *Atmosphere*, 10, 226, <https://doi.org/10.3390/atmos10040226>, 2019.

455 Johnston, M. V. and Kerecman, D. E.: Molecular Characterization of Atmospheric Organic Aerosol by Mass Spectrometry, *Annu. Rev. Anal. Chem.*, 12, 247-274, <https://doi.org/10.1146/annurev-anchem-061516-045135>, 2019.

Kalberer, M., Paulsen, D., Sax, M., Steinbacher, M., Dommen, J., Prevot, A. S. H., Fisseha, R., Weingartner, E., Frankevich, V., and Zenobi, R.: Identification of polymers as major components of atmospheric organic aerosols, *Science*, 303, 1659-1662, <https://doi.org/10.1126/science.1092185>, 2004.

460 Kuo, Y., Yang, T. and Huang, G.W.: The use of grey relational analysis in solving multiple attribute decision-making problems, 55, 80-93, *Comput. Ind. Eng.*, <https://doi.org/10.1016/j.cie.2007.12.002>, 2008.

Lakowicz, J. R.: *Principles of Fluorescence Spectroscopy*, Springer US. <https://doi.org/10.1007/978-0-387-46312-4>, 2006.

Lee, H. J., Aiona, P. K., Laskin, A., Laskin, J. and Nizkorodov, S. A.: Effect of solar radiation on the optical properties and molecular composition of laboratory proxies of atmospheric brown carbon, *Environ. Sci. Technol.*, 48, 10217-10226, <https://doi.org/10.1021/es502515r>, 2014.

465 Lee, H. J., Laskin, A., Laskin, J. and Nizkorodov, S. A.: Excitation-emission spectra and fluorescence quantum yields for fresh and aged biogenic secondary organic aerosols, *Environ. Sci. Technol.*, 47, 5763-5770, <https://doi.org/10.1021/es400644c>, 2013.

Liu, J., Bergin, M., Guo, H., King, L., Kotra, N., Edgerton, E. and Weber, R. J.: Size-resolved measurements of brown carbon in water and methanol extracts and estimates of their contribution to ambient fine-particle light absorption, *Atmos. Chem. 470 Phys.*, 13, 12389-12404, <https://doi.org/10.5194/acp-13-12389-2013>, 2013.

Masalaite, A., Holzinger, R., Ceburnis, D., Remeikis, V., Ulevicius, V., Rockmann, T. and Dusek, U.: Sources and atmospheric processing of size segregated aerosol particles revealed by stable carbon isotope ratios and chemical speciation, *Environ. Pollut.*, 240, 286-296, <https://doi.org/10.1016/j.envpol.2018.04.073>, 2018.

475 Mayorga, R. J., Zhao, Z. and Zhang, H.: Formation of secondary organic aerosol from nitrate radical oxidation of phenolic VOCs: Implications for nitration mechanisms and brown carbon formation, *Atmos. Environ.*, 244, 117910, <https://doi.org/10.1016/j.atmosenv.2020.117910>, 2021.

Morán, J., Granada, E., Míguez, J. L. and Porteiro, J.: Use of grey relational analysis to assess and optimize small biomass boilers, *Fuel. Process. Technol.*, 87, 123-127, <https://doi.org/10.1016/j.fuproc.2005.08.008>, 2006.

Murphy, K. R., Hambly, A., Singh, S., Henderson, R. K., Baker, A., Stuetz, R. and Khan, S. J.: Organic matter fluorescence
480 in municipal water recycling schemes: toward a unified PARAFAC model, *Environ. Sci. Technol.*, 45, 2909-2916,
<https://doi.org/10.1021/es103015e>, 2011.

Park S., Yu, J., Yu, G.-H. and 배민석: Chemical and absorption characteristics of water-soluble organic carbon and humic-like substances in size segregated particles from biomass burning emissions, *Asian J. Atmos. Environ.*, 11, 96-106,
<https://doi.org/10.5572/ajae.2017.11.2.096>, 2017.

485 Pohlker, C., Huffman, J. A. and Poschl, U.: Autofluorescence of atmospheric bioaerosols-fluorescent biomolecules and potential interferences, *Atmos. Meas. Tech.*, 5, 37-71, <https://doi.org/10.5194/amt-5-37-2012>, 2012.

Pósfai, M. and Buseck, P. R.: Nature and climate effects of individual tropospheric aerosol particles, *Annu. Rev. Earth. Pl. Sc.*, 38, 17-43, <https://doi.org/10.1146/annurev.earth.031208.100032>, 2010.

490 Qin, J., Zhang, L., Zhou, X., Duan, J., Mu, S., Xiao, K., Hu, J. and Tan, J.: Fluorescence fingerprinting properties for exploring water-soluble organic compounds in PM 2.5 in an industrial city of northwest China, *Atmos. Environ.*, 184, 203-211,
<https://doi.org/10.1016/j.atmosenv.2018.04.049>, 2018.

Qiu, B., Wang, F., Li, Y. and Zuo, W.: Research on method of simulation model validation based on improved grey relational analysis, *Phys. Pro.*, 25, 1118-1125, <https://doi.org/10.1016/j.phpro.2012.03.208>, 2012.

Santos, P. S. M., Duarte, R. and Duarte, A. C.: Absorption and fluorescence properties of rainwater during the cold season at
495 a town in Western Portugal, *J. Atmos. Chem.*, 62, 45-57, <https://doi.org/10.1007/s10874-009-9138-1>, 2009.

Stark, R. E., Yu, B., Zhong, J., Yan, B., Wu, G. and Tian, S.: Environmental NMR: High-resolution Magic-angle Spinning, 2,
377-388, <https://doi.org/10.1002/9780470034590.emrstm1340>, 2013.

Tan, J., Xiang, P., Zhou, X., Duan, J., Ma, Y., He, K., Cheng, Y., Yu, J. and Querol, X.: Chemical characterization of humic-like substances (HULIS) in PM_{2.5} in Lanzhou, China, *Sci Total Environ.*, 573, 1481-1490,
500 <https://doi.org/10.1016/j.scitotenv.2016.08.025>, 2016.

Tian, S., Pan, Y., Liu, Z., Wen, T. and Wang, Y.: Size-resolved aerosol chemical analysis of extreme haze pollution events during early 2013 in urban Beijing, China, *J Hazard Mater.*, 279, 452-460, <https://doi.org/10.1016/j.jhazmat.2014.07.023>, 2014.

Tian, S. L., Pan, Y. P. and Wang, Y. S.: Size-resolved source apportionment of particulate matter in urban Beijing during haze and non-haze episodes, *Atmos. Chem. Phys.*, 16, 1-19, <https://doi.org/10.5194/acp-16-1-2016>, 2016.

505 Vione, D., Albinet, A., Barsotti, F., Mekic, M., Jiang, B., Minero, C., Brigante, M. and Gligorovski, S.: Formation of substances with humic-like fluorescence properties, upon photoinduced oligomerization of typical phenolic compounds emitted by biomass burning, *Atmos. Environ.*, 206, 197-207, <https://doi.org/10.1016/j.atmosenv.2019.03.005>, 2019.

Voliotis, A., Prokeš, R., Lammel, G. and Samara, C.: New insights on humic-like substances associated with wintertime urban aerosols from central and southern Europe: Size-resolved chemical characterization and optical properties, *Atmos. Environ.*,
510 166, 286-299, <https://doi.org/10.1016/j.atmosenv.2017.07.024>, 2017.

Wang, H., Zhang, L., Huo, T., Wang, B., Yang, F., Chen, Y., Tian, M., Qiao, B. and Peng, C.: Application of parallel factor analysis model to decompose excitation-emission matrix fluorescence spectra for characterizing sources of water-soluble brown carbon in PM_{2.5}, *Atmos. Environ.*, 223, 117-192, <https://doi.org/10.1016/j.atmosenv.2019.117192>, 2020.

515 Wu, C., Wang, G., Li, J., Li, J., Cao, C., Ge, S., Xie, Y., Chen, J., Li, X., Xue, G., Wang, X., Zhao, Z. and Cao, F.: The characteristics of atmospheric brown carbon in Xi'an, inland China: sources, size distributions and optical properties, *Atmos. Chem. Phys.*, 20, 2017-2030, <https://doi.org/10.5194/acp-20-2017-2020>, 2020.

Xiang, P., Zhou, X. M., Duan, J. C., Tan, J. H., He, K. B., Yuan, C., Ma, Y. L. and Zhang, Y. X.: Chemical characteristics of water-soluble organic compounds (WSOC) in PM_{2.5} in Beijing, China: 2011-2012, *Atmos. Res.*, 183, 104-112, <https://doi.org/10.1016/j.atmosres.2016.08.020>, 2017.

520 Xiao, K., Han, B., Sun, J., Tan, J., Yu, J., Liang, S., Shen, Y. and Huang, X.: Stokes shift and specific fluorescence as potential indicators of organic matter hydrophobicity and molecular weight in membrane bioreactors, *Environ Sci Technol*, 53, 8985-8993, <https://doi.org/10.1021/acs.est.9b02114>, 2019.

Xiao, K., Shen, Y., Liang, S., Tan, J., Wang, X., Liang, P. and Huang, X.: Characteristic regions of the fluorescence excitation-emission matrix (EEM) to identify hydrophobic/hydrophilic contents of organic matter in membrane bioreactors, *Environ Sci 525 Technol*, 52, 11251-11258, <https://doi.org/10.1021/acs.est.8b02684>, 2018b.

Xiao, K., Sun, J.-Y., Shen, Y.-X., Liang, S., Liang, P., Wang, X.-M. and Huang, X.: Fluorescence properties of dissolved organic matter as a function of hydrophobicity and molecular weight: case studies from two membrane bioreactors and an oxidation ditch, *RSC Advances*, 6, 24050-24059, <https://doi.org/10.1039/C5RA23167A>, 2016.

530 Xiao, K., Yu, J., Wang, S., Du, J., Tan, J., Xue, K., Wang, Y. and Huang, X.: Relationship between fluorescence excitation-emission matrix properties and the relative degree of DOM hydrophobicity in wastewater treatment effluents, *Chemosphere*, 254, 126830, <https://doi.org/10.1016/j.chemosphere.2020.126830>, 2020.

Xie, X., Chen, Y., Nie, D., Liu, Y., Liu, Y., Lei, R., Zhao, X., Li, H. and Ge, X.: Light-absorbing and fluorescent properties of atmospheric brown carbon: A case study in Nanjing, China, *Chemosphere*, 251, 126350, <https://doi.org/10.1016/j.chemosphere.2020.126350>, 2020.

535 Xu, J. A., Sheng, G. P., Luo, H. W., Fang, F., Li, W. W., Zeng, R. J., Tong, Z. H. and Yu, H. Q.: Evaluating the influence of process parameters on soluble microbial products formation using response surface methodology coupled with grey relational analysis, *Water Res.*, 45, 674-680, <https://doi.org/10.1016/j.watres.2010.08.032>, 2011.

Yan, C., Nie, W., Vogel, A. L., Dada, L., Lehtipalo, K., Stolzenburg, D., Wagner, R., Rissanen, M. P., Xiao, M., Ahonen, L., Fischer, L., Rose, C., Bianchi, F., Gordon, H., Simon, M., Heinritzi, M., Garmash, O., Roldin, P., Dias, A., Ye, P., Hofbauer, 540 V., Amorim, A., Bauer, P. S., Bergen, A., Bernhammer, A.-K., Breitenlechner, M., Brilke, S., Buchholz, A., Mazon, S. B., Canagaratna, M. R., Chen, X., Ding, A., Dommen, J., Draper, D. C., Duplissy, J., Frege, C., Heyn, C., Guida, R., Hakala, J., Heikkinen, L., Hoyle, C. R., Jokinen, T., Kangasluoma, J., Kirkby, J., Kontkanen, J., Kürten, A., Lawler, M. J., Mai, H., Mathot, S., Mauldin, R. L., Molteni, U., Nichman, L., Nieminen, T., Nowak, J., Ojdanic, A., Onnela, A., Pajunoja, A., Petäjä, T., Piel, F., Quéléver, L. L. J., Sarnela, N., Schallhart, S., Sengupta, K., Sipilä, M., Tomé, A., Tröstl, J., Väisänen, O., Wagner,

545 A. C., Ylisirniö, A., Zha, Q., Baltensperger, U., Carslaw, K. S., Curtius, J., Flagan, R. C., Hansel, A., Riipinen, I., Smith, J. N., Virtanen, A., Winkler, P. M., Donahue, N. M., Kerminen, V.-M., Kulmala, M., Ehn, M. and Worsnop, D. R.: Size-dependent influence of NO_x on the growth rates of organic aerosol particles, *Sci. Adv.*, 6, eaay4945, <https://doi.org/10.1126/sciadv.aay4945>, 2020.

550 You, M. L., Shu, C. M., Chen, W. T. and Shyu, M. L.: Analysis of cardinal grey relational grade and grey entropy on achievement of air pollution reduction by evaluating air quality trend in Japan, *J. Clean Prod.*, 142, 3883-3889, <https://doi.org/10.1016/j.jclepro.2016.10.072>, 2017.

555 Yu, G. H., Park, S. and Lee, K. H.: Source contributions and potential source regions of size-resolved water-soluble organic carbon measured at an urban site over one year, *Environ. Sci. Process. Impacts.*, 18, 1343-1358, <https://doi.org/10.1039/c6em00416d>, 2016.

560 Yu, J. Z., Yang, H., Zhang, H. Y. and Lau, A. K. H.: Size distributions of water-soluble organic carbon in ambient aerosols and its size-resolved thermal characteristics, *Atmos. Environ.*, 38, 1061-1071, <https://doi.org/10.1016/j.atmosenv.2003.10.049>, 2004.

565 Yu, Q., Chen, J., Qin, W., Cheng, S., Zhang, Y., Ahmad, M. and Ouyang, W.: Characteristics and secondary formation of water-soluble organic acids in PM₁, PM_{2.5} and PM₁₀ in Beijing during haze episodes, *Sci. Total. environ.*, 669, 175-184, <https://doi.org/10.1016/j.scitotenv.2019.03.131>, 2019.

570 Yue, S., Ren, L., Song, T., Li, L., Xie, Q., Li, W., Kang, M., Zhao, W., Wei, L., Ren, H., Sun, Y., Wang, Z., Ellam, R. M., Liu, C. Q., Kawamura, K. and Fu, P.: Abundance and Diurnal Trends of Fluorescent Bioaerosols in the Troposphere over Mt. Tai, China, in Spring, *J. Geophys. Res.-Atmos.*, 124, 4158-4173, <https://doi.org/10.1029/2018jd029486>, 2019.

575 Zanca, N., Lambe, A. T., Massoli, P., Paglione, M., Croasdale, D. R., Parmar, Y., Tagliavini, E., Gilardoni, S. and Decesari, S.: Characterizing source fingerprints and ageing processes in laboratory-generated secondary organic aerosols using proton-nuclear magnetic resonance (¹H-NMR) analysis and HPLC HULIS determination, *Atmos. Chem. Phys.*, 17, 10405-10421, <https://doi.org/10.5194/acp-17-10405-2017>, 2017.

580 Zhang, X., Liu, Z., Hecobian, A., Zheng, M., Frank, N. H., Edgerton, E. S., Weber, R. J.: Spatial and seasonal variations of fine particle water-soluble organic carbon (WSOC) over the southeastern United States: implications for secondary organic aerosol formation, *Atmos. Chem. Phys.*, 12, 6593-6607, <https://doi.org/10.5194/acp-12-6593-2012>, 2012.

585 Zhang, X., Xu, J., Kang, S., Liu, Y. and Zhang, Q.: Chemical characterization of long-range transport biomass burning emissions to the Himalayas: insights from high-resolution aerosol mass spectrometry, *Atmos. Chem. Phys.*, 18, 4617-4638, <https://doi.org/10.5194/acp-18-4617-2018>, 2018.

590 Zhao, W., Fu, P., Yue, S., Li, L., Xie, Q., Zhu, C., Wei, L., Ren, H., Li, P., Li, W., Sun, Y., Wang, Z., Kawamura, K. and Chen, J.: Excitation-emission matrix fluorescence, molecular characterization and compound-specific stable carbon isotopic composition of dissolved organic matter in cloud water over Mt. Tai, *Atmos. Environ.*, 213, 608-619, <https://doi.org/10.1016/j.atmosenv.2019.06.034>, 2019.

Table 1 Size segregated average WSOC, WSIN concentrations, and their standard deviations.

	Species (mg·m ⁻³)	<0.26 μm	0.26-0.44μm	0.44-0.77μm	0.77-1.4μm	1.4-2.5μm	2.5-10 μm
Winter	Cl ⁻	0.42±0.25	1.36±1.21	0.83±0.72	1.03±0.98	1.19±1.27	0.43±0.45
	NO ₃ ⁻	2.08±1.43	9.42±8.46	5.64±5.61	7.37±8.9	6.72±9.44	1.92±3.28
	SO ₄ ²⁻	1.05±0.6	4.36±3.87	3.21±3.68	5.44±9.43	4.68±7.03	1.18±1.52
	Na ⁺	0.12±0.05	0.21±0.1	0.16±0.08	0.2±0.1	0.52±0.6	0.24±0.25
	NH ₄ ⁺	1.05±0.57	2.9±2.15	2.05±1.82	2.4±2.77	1.67±2.18	0.44±0.67
	Mg ²⁺	0.01	0.01	0.02±0.01	0.05±0.04	0.18±0.21	0.08±0.09
	Ca ²⁺	0.06±0.01	0.11±0.03	0.15±0.08	0.4±0.25	1.67±1.35	0.93±0.9
	K ⁺	0.08±0.04	0.37±0.3	0.24±0.24	0.25±0.25	0.18±0.18	0.05±0.06
	OC	4.49±1.93	11.04±7.2	5.67±4.49	5.45±6.26	5.07±3.88	3.4±5.17
	EC	0.38±0.18	0.93±0.47	0.67±0.43	0.72±0.69	0.62±0.78	1.65±4.37
Summer	WSOC	1.66±0.7	4.73±2.96	2.96±2.41	3.21±4.33	2.31±2.55	0.64±0.5
	WSOC/OC	0.38±0.07	0.43±0.07	0.56±0.27	0.51±0.15	0.37±0.14	0.24±0.25
	Cl ⁻	0.05±0.02	0.1±0.04	0.07±0.03	0.07±0.02	0.16±0.1	0.11±0.06
	NO ₃ ⁻	0.48±0.44	3.5±3.32	1.37±1.35	1.04±0.86	4.76±4.22	1.49±1.37
	SO ₄ ²⁻	1.63±1.18	7.14±6.64	2.59±2.42	1.28±1.13	0.72±0.51	0.2±0.12
	Na ⁺	0.29±0.08	0.37±0.17	0.25±0.06	0.23±0.06	0.27±0.09	0.19±0.03
	NH ₄ ⁺	0.79±0.53	2.56±1.99	1.18±1.02	0.63±0.55	0.5±0.46	0.1±0.08
	Mg ²⁺	0.01	0.01	0.01	0.02±0.01	0.12±0.08	0.05±0.03
	Ca ²⁺	0.05±0.01	0.08±0.02	0.08±0.03	0.16±0.09	1.21±0.87	0.62±0.49
	K ⁺	0.03±0.02	0.14±0.11	0.05±0.04	0.04±0.02	0.06±0.02	0.02±0.01
OC	2.67±0.98	3.93±2.22	1.39±0.67	1.14±0.41	3.5±1.21	2.22±1.76	
	EC	0.38±0.12	0.44±0.16	0.2±0.09	0.22±0.06	0.34±0.22	0.5±0.52
	WSOC	0.67±0.25	1.27±0.86	0.46±0.31	0.33±0.21	0.57±0.18	0.27±0.18
	WSOC/OC	0.26±0.08	0.3±0.07	0.31±0.1	0.27±0.1	0.17±0.04	0.16±0.12

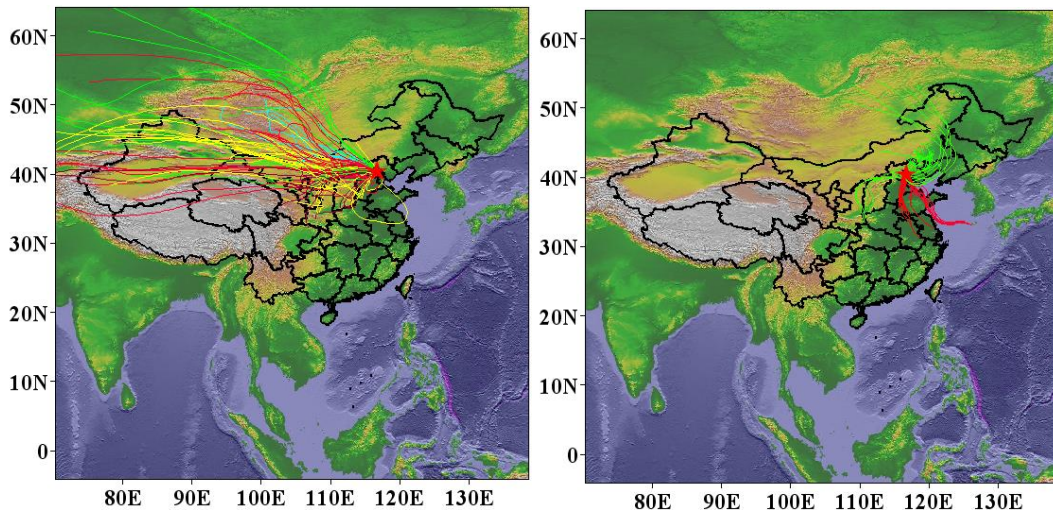


Figure 1 The sampling site and air quality index (AQI) weighted 72 h backward trajectory of winter and summer sampling days, respectively.

585

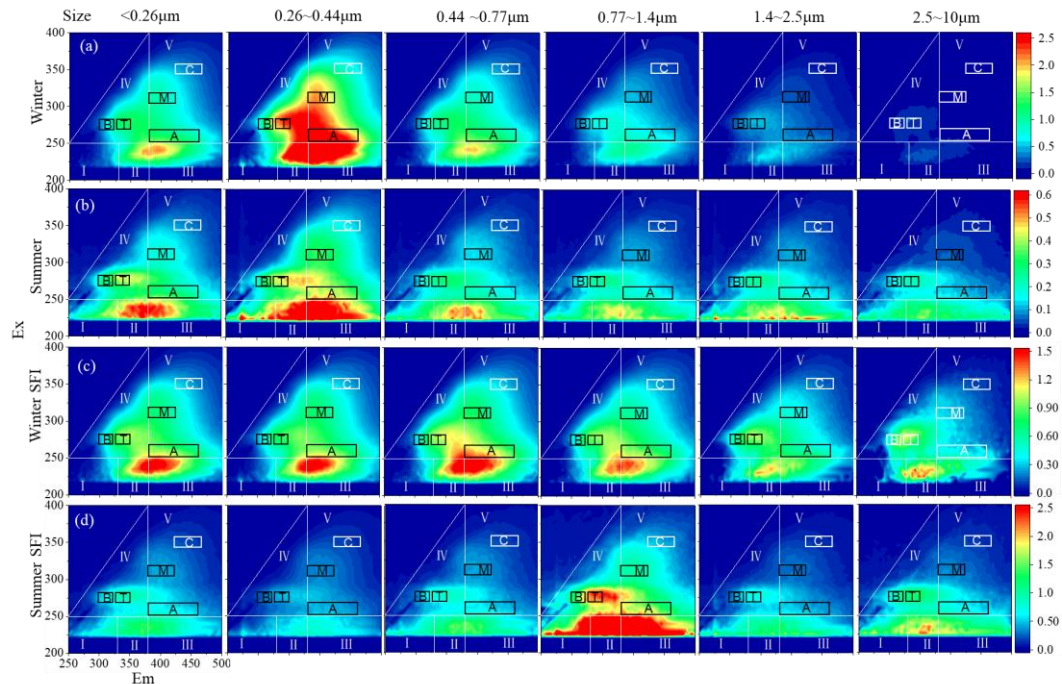
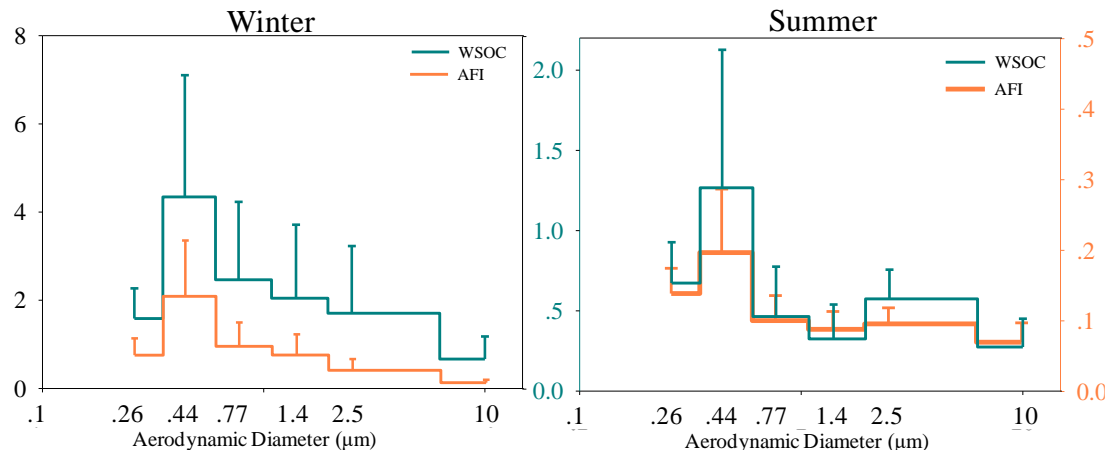


Figure 2 Excitation-emission spectra of size segregated samples in winter and summer. All spectra were partitioned into five regions and assigned as protein-like pollutants (I and II), fulvic acid (III), soluble microbial byproduct-like substances (IV), and humic-like acid (V), respectively (Birdwell and Engel 2010). Peak A, B, C, M, and T were generally considered as humic-like fluorophores, tyrosine-like fluorophores, humic-like carbon with larger molecular weight, marine humic-like fluorophore, and tryptophan-like fluorophores (Coble 1996). (a) and (b) were the size segregated

590

EEM spectra of winter and summer samples, respectively (R.U.), (c), and (d) were the corresponding EEM spectra of fluorescence emitted per unit of WSOC.



595 **Figure 3 Size distributions of WSOC and AFI in winter and summer. AFI was in the Raman unit.**

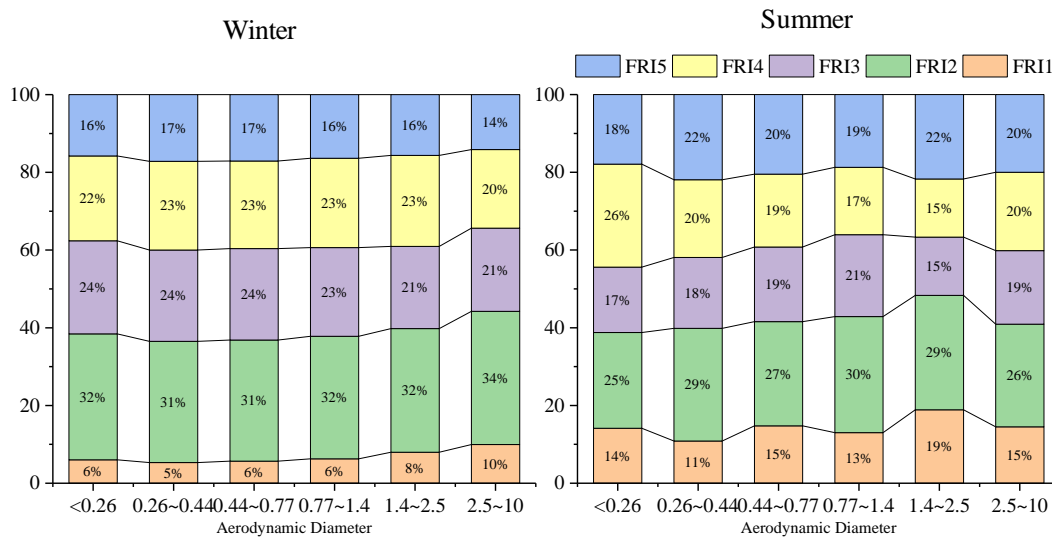
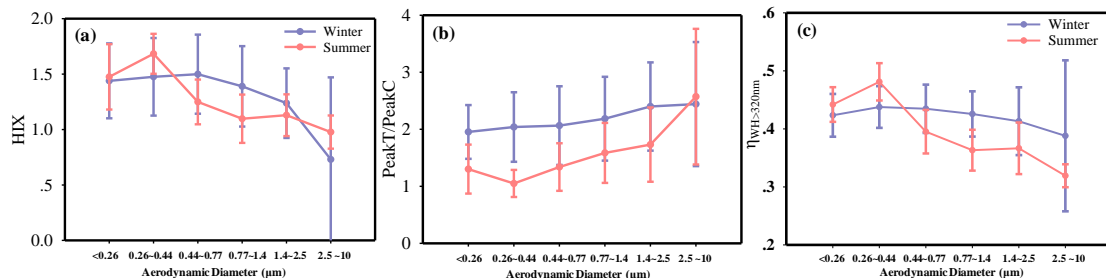
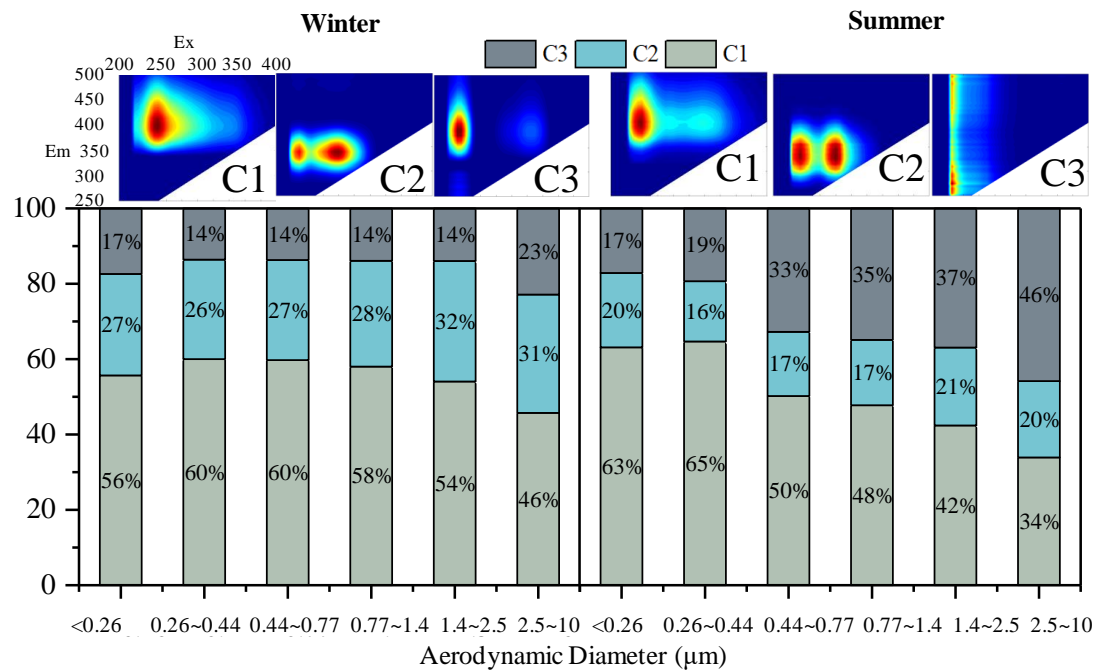


Figure 4 Size distribution of fluorescence regional intensity for winter and summer. FRI1-FRI5 was FRI of fluorescence region I to V.



600 **Figure 5** Humic index and Peak T/Peak C ratio served as indicators of humification degree and the biodegradable possibility of WSOC. (a) HIX in different particle sizes, large HIX value indicated high humification degree or high aromaticity of fluorescent organics. (b) Peak T/Peak C ratios of different particle sizes. The large value indicated more microbial metabolites in the fluorescent organics. (c) showed the size distributions of $\eta_{WH>320}$ for winter and summer samples, respectively.



605 **Figure 6** PARAFAC results of EEM in winter and summer respectively. Three components were extracted of both seasons, the portions of each component for different particle sizes were shown as well.

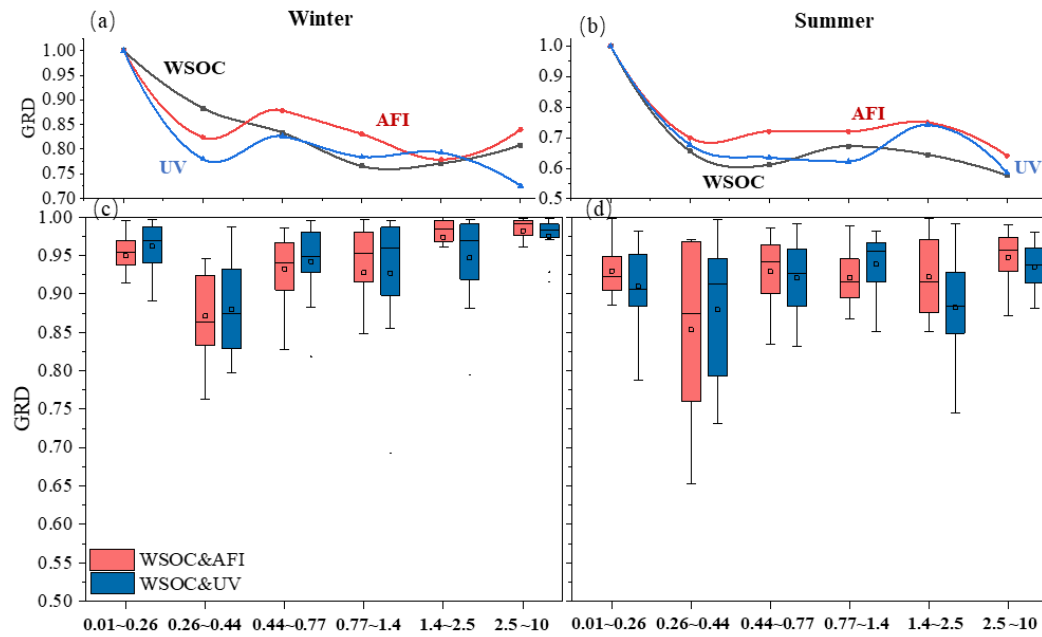


Figure 7 Grey relational degree (GRD) of size segregated WSOC, AFI, and average UV. (a) and (b) GRD calculated by WSOC, AFI, and average UV of each sample, setting data of 0.01 to 0.26 as references, GRD (0.01-0.26) = 1; (c) and (d) GRD between WSOC and light absorption indices, setting WSOC as references.